

Tuning the Kosterlitz-Thouless transition to zero temperature in Anisotropic Boson Systems

Jhih-Shih You^{1,2}, Hao Lee^{1,2}, Shiang Fang^{1,2}, Miguel A. Cazalilla^{3,4,5}, Daw-Wei Wang^{1,2}

¹ *Physics Department and Frontier Research Center on Fundamental and Applied Sciences of Matter, National Tsing-Hua University, Hsinchu, Taiwan*

² *Physics Division, National Center for Theoretical Sciences, Hsinchu, Taiwan*

³ *Centro de Física de Materiales CSIC-UPV/EHU. Paseo Manuel de Lardizabal 5, E-20018 San Sebastian, Spain*

⁴ *DIPC, Paseo Manuel de Lardizabal 4, E-20018 San Sebastian, Spain*

⁵ *Graphene Research Centre National University of Singapore, 6 Science Drive 2, Singapore 117546.*

(Dated: July 10, 2012)

We study the two-dimensional Bose-Hubbard model with anisotropic hopping. Focusing on the effects of anisotropy on the superfluid properties such like the helicity modulus and the normal-to-superfluid (Berezinskii-Kosterlitz-Thouless, BKT) transition temperature, two different approaches are compared: Large-scale Quantum Monte Carlo simulations and the self-consistent harmonic approximation (SCHA). For the latter, two different formulations are considered, one applying near the isotropic limit and the other applying in the extremely anisotropic limit. Thus we find that the SCHA provides a reasonable description of superfluid properties of this system provided the appropriate type of formulation is employed. The accuracy of the SCHA in the extremely anisotropic limit, where the BKT transition temperature is tuned to zero (i.e. into a Quantum critical point) and therefore quantum fluctuations play a dominant role, is particularly striking.

I. INTRODUCTION

In recent years, much progress has been made in ultracold atoms loaded in optical lattices.^{1–3} Several experimental groups have demonstrated the large tunability of such systems by driving them from a superfluid to a Mott insulator phase (and vice versa) in various dimensions and lattice geometries.^{1,4–9} By varying the laser intensity along one or several directions, experimentalists can control the hopping anisotropy for the atoms in the optical lattice.^{4,5,8,10} Thus, some of these experiments have started to explore the fascinating behavior of ultracold atoms confined to low dimensions.^{4,5,8,10} This control makes it also possible to study dimensional crossovers^{4,11–14} as well as a wide range of other phenomena,^{4,8} which are also relevant for the understanding of complex solid-state systems such as layered superconductors^{15–18} and anisotropic magnetic materials.^{19–22}

Indeed, matter in low dimensions is known to dis-

play a wide range exotic properties, which are otherwise hard to come across in three dimensional systems. These include fractionalization of quantum numbers,²³ critical states lacking long range order,^{4,8,10,24} and topological phase transitions that cannot be characterized by an order parameter such as the Berezinskii-Kosterlitz-Thouless (BKT) transition.^{10,25,26} The question of how these exotic properties evolve as low-dimensional systems are coupled and become, by virtue of the coupling, higher dimensional systems has attracted a great deal of experimental and theoretical attention in recent years.^{4,11–14,21,22,24,27–29}

In bosonic systems, such as ultracold gases of bosonic atoms or molecules, as well as in anisotropic magnetic materials,²⁴ a theoretical analysis of the dimensional crossovers and other interesting phenomena such as deconfinement transitions^{13,14} can be carried out through a combination of perturbative renormalization-group (RG) and mean-field theory (MFT) approaches. MFT assumes the existence of a Bose-Einstein condensate and it is expected to be a reliable description of the anisotropic superfluid phase only if the crossover takes place from one to three dimensions. However, when trying to describe the crossover from one (1D) to two dimensions (2D) at finite temperatures, MFT breaks down because bosons in two dimensions fail to condense at all temperatures except at $T = 0$. Nevertheless, under such conditions a qualitative understanding of the properties of the anisotropic superfluid phase can be still obtained by means of perturbative RG and variational methods, as we shall demonstrate below. However, an independent check of these approximated methods is still required.

It is worth noting that the superfluid properties appear to be strongly dependent on the system dimensionality.^{26,30–34} Experimentally, a superfluid response has been observed at finite temperatures in both two-²⁶ and

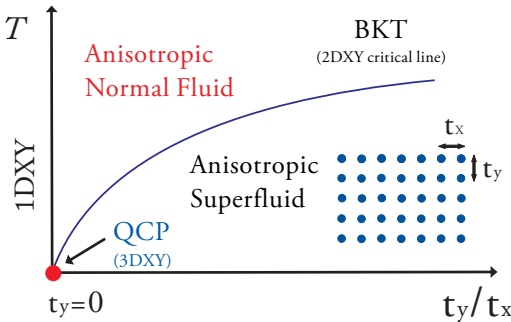


FIG. 1: Schematic Phase Diagram for the Bose-Hubbard model with hopping anisotropy ratio in two dimensions.

one-dimensional³⁰ interacting boson systems, which lack of a Bose-Einstein condensate. However, the origin of the superfluidity in these two cases is very different:^{31,34} Whereas in 2D the superfluid response is essentially a thermodynamic phenomenon that is quantified by the helicity modulus,³¹ in 1D it is a dynamic property as the helicity modulus vanishes at all temperatures (the helicity modulus at zero temperature is obtained by taking the $T \rightarrow 0$ limit *after* taking the thermodynamic limit^{32,34}). The vanishing helicity modulus of the 1D Bose fluid is in stark contrast with the universal jump exhibited by the helicity modulus across the BKT transition. As it will be discussed below, making the hopping amplitude in one direction vanishingly small, drives the BKT transition temperature to the absolute zero (at $T = 0$) and the transition thus becomes a 3DXY quantum critical point (QCP) at the end of a line of classical 2DXY critical points (cf. Fig 1). This critical line separates the anisotropic normal and superfluid phases. Therefore, it can be argued that the helicity modulus vanishes in 1D Bose fluids because these fluids share the same superfluid properties as the *normal* fluid phase in the limit of vanishing anisotropy ratio. This can be seen by noticing the the helicity modulus of the 1D Bose fluid can be obtained by approaching the 1D limit along a finite temperature (i.e. $T > 0$) trajectory (cf. Fig. 1), which means no critical line is crossed for sufficiently small starting anisotropy ratio. On the other hand, approaching the 1D limit along the $T = 0$ line necessarily implies reaching the QCP first, which is a thermodynamic singularity (cf. Fig 1).

Indeed, the variety of phenomena that can be studied in anisotropic bosonic systems is very wide.^{13,14,24} In this work, we focus on understanding the properties of the anisotropic superfluid phase that can be realized in e.g. two-dimensional optical lattices with hopping anisotropy. However, our results can be also of relevance to much more complex solid-state systems, such like anisotropic magnetic insulators.^{21,22,24} In particular, we are interested in understanding how the hopping anisotropy affects the properties of the superfluid phase (i.e. the helicity modulus) and the Berezinskii-Kosterlitz-Thouless (BKT) transition temperature from the superfluid to the normal fluid phase. As the BKT transition temperature is tuned towards $T = 0$ by the hopping anisotropy, the importance of quantum fluctuations is enhanced. Thus, we expect that this will lead to important renormalization effects on the parameters of the effective 2DXY model that describes the line of classical critical points. Below we shall rely on the self-consistent harmonic approximation (SCHA) to various limits of the quantum rotor model to estimate such renormalization effects. The results of the calculations based on the SCHA for the critical temperature and the helicity modulus will be compared with Quantum Monte Carlo simulations.

Of course, the effect of quantum fluctuations is enhanced not only by the anisotropy but also by the inter-particle interaction, which can drive a quantum phase transition from the superfluid phase to a Mott insu-

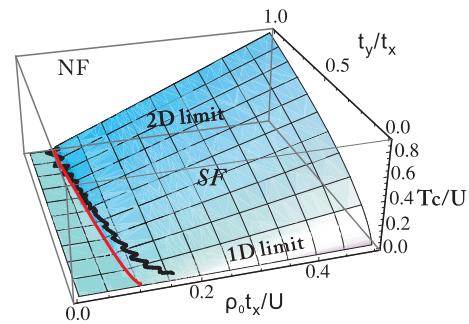


FIG. 2: The complete phase diagram of an anisotropic Hubbard model as a function of anisotropy ratio, t_y/t_x , interaction strength, $\rho_0 t_x/U$, and temperature, T/U . Note that we keep U to be a constant and vary other quantities for convenience. This is calculated by SCHA as described in the text. The red line guides zero temperature transitions (from superfluid to Mott insulator phase), while the black line is calculated by QMC at very low temperature ($T/U = 0.01$) for comparison. Here we set chemical potential $\mu/U = 0.375$ (the mean boson occupation $\rho_0 \sim 1$) to get the QMC results.

lator phase at integer fillings. In various dimensions, such superfluid-to-Mott insulator transition has been extensively studied both experimentally and theoretically, mainly in isotropic systems^{1,4-9}. However, the combined effect of anisotropy and inter-particle interactions in enhancing the quantum fluctuations and destroying superfluidity in two dimensional Bose systems has not been studied so far. In this paper, we shall show how both quantum and thermal fluctuations can be treated on equal footing in the study of anisotropic superfluid in a 2D optical lattice. Our results can be summarized in the phase diagram shown in Fig. 2.

The outline of this article is as follows: In section II we introduce the relevant low energy models that we use to describe the anisotropic Bose-Hubbard model (BHM) in 2D. Several analytic and numerical approximations to the BHM are also discussed there. We also discuss the problem of how to estimate the “phase-stiffness” parameters of the 2DXY model that describes the critical line of BTK transitions separating the normal and superfluid phases at finite temperature (cf. Figs. 1,2). In section III, the effects of thermal fluctuations and interaction on helicity modulus from small to intermediate anisotropy are discussed. In section IV we explore these renormalization effects in the extremely anisotropic regime, as well as the behavior of the BKT critical temperature. The conclusions of this work can be found in section V. The appendixes contain the technical details of SCHA calculations in the various limits of the quantum rotor model.

II. MODELS AND METHODS

The anisotropy of the single particle tunneling can be easily realized in an optical lattice by using different laser

intensities for the standing waves in the x and y directions. In the limit of a deep lattice, in which essentially all particles reside in the lowest Bloch band, the system can be described by the single-band Bose Hubbard model:

$$H = - \sum_{\langle i,j \rangle} t_{ij} b_i^\dagger b_j - \mu \sum_i \hat{n}_i + \frac{U}{2} \sum_i n_i(n_i - 1) \quad (1)$$

where b_i^\dagger is bosonic creation operator on site \mathbf{R}_i , and $n_i = b_i^\dagger b_i$ is boson occupation operator. The tunneling amplitude is $t_{ij} = t_x$ ($t_{ij} = t_y$), if $\mathbf{R}_i - \mathbf{R}_j = \pm a \hat{x}$ ($\mathbf{R}_i - \mathbf{R}_j = \pm a \hat{y}$) with a being the lattice constant. U and μ are the on-site interaction and chemical potential, respectively.

A. The XY Model and the Self-consistent Harmonic Approximation (SCHA)

Deep into the superfluid phase, the low-temperature behavior of the system is largely dominated by phase fluctuations. For a sufficiently large values of U and for the *bare* anisotropy ratio parameter $\eta_0 = J_y^0/J_x^0 \approx 1$, we can represent the boson operator as $b_i = \sqrt{\rho_0 + \delta\rho_i} e^{i\theta_i}$, where ρ_0 is the mean boson occupation, while θ_i and $\delta\rho_i$ ($\ll \rho_0$) describe the phase and density fluctuations at site \mathbf{R}_i , respectively. After integrating out the density fluctuations, the partition function (Z) of the system can be written as a (Feynman) functional integral, $Z = \int \mathcal{D}\theta e^{-S_{\text{XY}}[\theta]}$, where ($\hbar = 1$)

$$S_{\text{XY}}[\theta] = \int_0^\beta d\tau \left[\sum_i \frac{(\partial_\tau \theta_i)^2}{2U} - \sum_{\langle i,j \rangle} 2J_{ij}^0 \cos(\theta_i - \theta_j) \right] \quad (2)$$

is the two-dimensional $O(2)$ quantum rotor model, with $J_{ij}^0 = \rho_0 t_{ij}$ being the *bare* Josephson coupling and $\beta = 1/T$ the inverse of the absolute temperature in units where the Boltzmann constant $k_B = 1$.

At sufficiently high temperatures, the imaginary time (τ) dependence of the phase θ_i can be neglected and the model in Eq. (2) becomes the classical ferromagnetic XY model:

$$S_{\text{C-XY}}[\theta] = -2\beta \sum_{\langle i,j \rangle} J_{ij}^0 \cos(\theta_i - \theta_j). \quad (3)$$

In 2D this model has two distinct phases: in the high temperature regime, the orientation of the rotors described by the phase θ_i is disordered. The phase correlations are short ranged, i.e. $g_{ij} = \langle e^{i\theta_i} e^{-i\theta_j} \rangle \simeq e^{-|\mathbf{R}_i - \mathbf{R}_j|/\xi(T)}$, where the correlation length $\xi(T) \gg a$. Such behavior corresponds to a normal phase. On the other hand, in the low temperature regime, the phase correlations decay algebraically, i.e. $g_{ij} \simeq |\mathbf{R}_i - \mathbf{R}_j|^{-\alpha(T)}$, where the exponent $\alpha(T)$ is finite and related to the thermodynamic phase stiffness. This behavior corresponds to a superfluid phase exhibiting quasi-long range order. The

latter implies the absence of a Bose-Einstein condensate, but the finite phase stiffness (J_{ij}^0) means that the system can sustain superflows at all temperatures below the Berezinskii-Kosterlitz-Thouless (BKT) temperature, T_c . Above such temperature, vortices and anti-vortices unbind and destroy the superfluid properties of the system. The vortices (anti-vortices) are singular configurations of the phase θ_i , where the latter winds out by positive (negative) integer multiples of 2π around a discrete set of points on the plane.

The picture described above relies on the classical (high temperature) limit of the quantum rotor model, where the first term in Eq. (2) ($\propto (\partial_\tau \theta_i)^2$) is neglected. In other words, if we expand

$$\theta_i(\tau) = \frac{1}{\beta} \sum_{\omega_n} e^{-i\omega_n \tau} \theta_i(\omega_n), \quad (4)$$

where $\omega_n = \frac{2\pi}{\beta} n$ (n being an integer), the high temperature limit only takes into account the fluctuations of the $\theta_i(\omega_n)$ field for $\omega_n = 0$. However, the model in Eq. (2) is quantum mechanical, and the quantum fluctuations are described by the finite Matsubara frequency (i.e. $\omega_n \neq 0$) components of $\theta_i(\omega_n)$. The latter and the classical (i.e. thermal) configurations described by $\theta_i(\omega_n = 0)$ are coupled non-linearly through the Josephson coupling term $\propto J_{ij}^0 \cos(\theta_i(\tau) - \theta_j(\tau))$. At low temperatures, both quantum and classical fluctuations must be taken into account. This means that we must obtain the effective classical limit of the quantum rotor model by integrating out the quantum fluctuations described by the $\theta_i(\omega_n \neq 0)$ components of the phase. This is especially important for the anisotropic XY model because, as we drive the system towards the extremely anisotropic limit where $t_y/t_x \ll 1$, the BKT transition temperature T_c tends to zero (cf. Figs. 1 and 2).

In order to carry out the integration of the quantum fluctuations, we shall rely upon the self-consistent harmonic approximation (SCHA).^{13,35} Thus, we shall assume that, below T_c , the quantum rotor model of Eq. 2 can be approximated by an anisotropic Gaussian model:

$$S_G[\theta] = \int_0^\beta d\tau \left[\sum_i \frac{(\partial_\tau \theta_i)^2}{2U} + \sum_{\langle i,j \rangle} J_{ij} (\theta_i - \theta_j)^2 \right] \quad (5)$$

where J_{ij} is the effective Josephson coupling renormalized by the interactions and the thermal fluctuations. The derivation of a self-consistent equation for J_{ij} is given in Appendix A.

B. Josephson Coupled Tomonaga-Luttinger Liquids and SCHA

For small values of the anisotropy ratio (i.e. for $t_y/t_x \rightarrow 0$), it is convenient to consider a different limit of the anisotropic Bose-Hubbard model introduced in Eq. (1).

Indeed, for $t_y = 0$, Eq. (1) reduces to an array of uncoupled 1D Bose gases. For temperatures $T \ll t_x$, an interacting 1D Bose gas is known to behave as a Tomonaga-Luttinger liquid (TLL).²⁴ Upon restoring a small $t_y (\ll t_x)$ coupling between the TLLs, the resulting system is an array of weakly coupled TLLs, which is described by the following effective Hamiltonian:^{14,24}

$$H_{\text{CTLL}} = \frac{v}{2\pi} \sum_{i=1}^{L_y} \int dx \left[K (\partial_x \theta_i)^2 + K^{-1} (\partial_x \phi_i)^2 \right] - \frac{g_J^0 v}{\pi a_0^2} \sum_{i=1}^{L_y} \int dx \cos[\theta_i - \theta_{i+1}], \quad (6)$$

where v is the sound velocity, K is the Luttinger parameter characterizing the decay of correlations, $a_0 \approx a$ is short-range cutoff, and $g_J^0 \simeq 2\pi t_y \rho_0 a_0^2 / v$. The fields $\frac{1}{\pi} \partial_x \phi_i(x)$ and $\theta_i(x)$ describe the (long wavelength) density and phase fluctuations of the 1D interacting Bose gas at site $i = 1, \dots, L_y$ of the array.

In order to obtain a phase-only description, we integrate out the density fields $\phi_i(x)$ in Eq.(6) and thus obtain the following action for the array of weakly coupled TLLs:

$$S_{\text{CTLL}}[\theta_i] = \frac{K}{2\pi} \sum_{i=1}^{L_y} \int_0^\beta d\tau \int_0^{L_x} dx \left[\frac{(\partial_\tau \theta_i)^2}{v} + v (\partial_x \theta_i)^2 \right] - \frac{g_J^0 v}{\pi a_0^2} \sum_{i=1}^{L_y} \int_0^\beta d\tau \int_0^{L_x} dx \cos(\theta_i - \theta_{i+1}), \quad (7)$$

It is now possible to apply the SCHA to this model by approximating the non-linear Josephson coupling in $S_{\text{TLL}}[\theta_i]$ by a Gaussian coupling:

$$S_G[\theta_i] = \frac{K}{2\pi} \sum_{i=1}^{L_y} \int_0^\beta d\tau \int_0^{L_x} dx \left[\frac{(\partial_\tau \theta_i)^2}{v} + v (\partial_x \theta_i)^2 \right] + \frac{g_J v}{\pi a_0^2} \sum_{i=1}^{L_y} \int_0^\beta d\tau \int_0^{L_x} dx (\theta_i - \theta_{i+1})^2, \quad (8)$$

where g_J is the effective SCHA coupling. It can be computed by solving the equation in Appendix B.

C. BKT Transition and The sine-Gordon Model

The advantage of the Gaussian models (either (5) or (8)), obtained after the application of the SCHA approximation, is that they allow for readily integrating out the "quantum components" of the phase field (i.e. the $\omega_n \neq 0$ components of θ). We can thus obtain, in the continuum limit where the variation of the phase is slow over the scale of the lattice parameter, a classical Gaussian model

$$S_{\text{C-G}}[\theta] = \frac{1}{2} \int dx dy \left[K_x (\partial_x \theta)^2 + K_y (\partial_y \theta)^2 \right], \quad (9)$$

where the expressions for stiffnesses K_x and K_y depend on the starting Gaussian model: $K_x = \beta J_x$ and $K_y = \beta J_y$, for Eq. (5), and $K_x = \beta K v / (a\pi)$ and $K_y = \beta g_J / (a\pi)$, for Eq. (8). Interestingly enough, the role of the anisotropy in the continuum limit description based on (9) seems to be rather minor. This can be seen by rescaling the coordinates $x \rightarrow \eta^{1/2} x$ and $y \rightarrow \eta^{-1/2} y$, where $\eta = \sqrt{K_x / K_y}$, yielding the following isotropic Gaussian model:

$$S_{\text{C-G}}[\theta] = \frac{K_\beta}{2} \int d\mathbf{r} (\nabla \theta)^2, \quad (10)$$

where $K_\beta = \sqrt{K_x K_y}$. Note that, in a finite system, the rescaling also affects the system dimensions: $L_x \rightarrow L_x \eta^{1/2}$ and $L_y \rightarrow L_y \eta^{-1/2}$. This observation will be important below.

Eq. (10) can be regarded as the *naïve* continuum limit of Eq.(3) and it can only describe the (thermal) phase fluctuations within the superfluid phase of Eq. (1). Thus, this model can only capture the algebraically decaying phase correlations characterizing the superfluid phase of the XY model (cf. Sec. II A). However, it is completely unable to capture the vortex and anti-vortex unwinding that ultimately drives the BKT transition.

In order to capture the possibility of topological excitations that ultimately lead to the BKT transition, we need to take a step back to the original XY model, either Eq. (2) or Eq. (7), and acknowledge that by relying on the SCHA, since we have neglected the possibility of topological configurations of the phase where the latter jumps by multiples of 2π from a given lattice site to a neighboring site. Thus, the right way to proceed would have been to start from the quantum XY model (or better, from the Bose-Hubbard model of Eq. (1)) and, after integrating out the quantum components of the phase (and density) fields, to arrive at an effective classical XY model like Eq. (3), with properly renormalized parameters. The latter, via a duality transformation,^{36,37} can be mapped onto the sine-Gordon model,

$$S_{\text{sG}} = \int d\mathbf{r} \left\{ \frac{[\nabla \phi(\mathbf{r})]^2}{2K_\beta^{(0)}} - \frac{2g^{(0)}}{a^2} \cos 2\pi \phi(\mathbf{r}) \right\}, \quad (11)$$

where $\phi(\mathbf{r})$ is a field that is dual^{36,37} to $\theta(\mathbf{r})$ and $g^0 \propto e^{-E_c/k_B T}$ is the so-called vortex fugacity with E_c being the vortex core energy. The classical 2DXY and the sine-Gordon models belong to the same universality class, which means that, near the BKT transition they provide an equally accurate description of the long-wave length phenomena. For the 2DXY universality class, Nelson and Kosterlitz have shown³¹ using the renormalization group (RG) that, at the critical temperature for the BKT transition, T_c , the *renormalized* phase-stiffness ($K_\beta^{(R)}$) exhibits a universal jump:

$$K_\beta^{(R)}(T \rightarrow T_c^-) = \frac{2}{\pi}, \quad (12)$$

$$K_\beta^{(R)}(T \rightarrow T_c^+) = 0. \quad (13)$$

The renormalized stiffness $K_\beta^{(R)}$ satisfies a set of differential RG equations, which describe the ‘flow’ of the sine-Gordon parameters (which correspond to $K_\beta^{(0)}$ and $g^{(0)}$ at the scale of the lattice parameter a) as the system *classical* degrees of freedom are coarse-grained in the vicinity of the BKT transition. Thus, RG equations determine the long wavelength properties of the system, or, in other words, the phase of system: For $K_\beta^{(R)} > 2/\pi$ (i.e for $T < T_c$), the coupling of the non-linear term ($\propto \cos 2\pi\phi$) in Eq. (11), which is responsible for the creation of vortex-anti-vortex pairs, is renormalized down to zero, leading us back to the Gaussian model (cf. Eq. 10) that describes the superfluid phase, but with a renormalized value of the stiffness equal to $K_\beta^{(R)}$. On the other hand, when $K_\beta^{(R)} < 2/\pi$ (for $T > T_c$), the vortex-anti-vortex pairs unbind, which means that the coefficient of the $\cos 2\pi\phi$ term grows as the system is coarse grained. The unbinding disorders the system thus destroying the superfluidity (i.e. $K_\beta^{(R)} \rightarrow 0$), and thus the system becomes a normal Bose fluid.

However, it must be pointed out that the derivation of the sine-Gordon model from the original Bose-Hubbard model (cf. Eq. 1) or the quantum XY model, Eq. (2) is very hard to carry out in practice. The reason is that the integration of the $\omega_n \neq 0$ components of the phase cannot be performed exactly due to the non-linear nature of the Josephson coupling. Thus, in this work we have chosen an alternative route, which involves using the SCHA to obtain the Gaussian model with effective parameters, K_x and K_y , from which we can obtain an *approximation* to the renormalized stiffness at T_c : $K_\beta^R(T_c) \approx K_\beta(T_c) = \sqrt{K_x(T_c)K_y(T_c)}$. As we shall show below by explicit comparison with QMC results, the SCHA provides a reasonably accurate estimate of the superfluid parameters even in an anisotropic Bose system where T_c is driven to zero. Within this framework, an approximation to the critical temperature is determined from the condition that

$$K_\beta(T_c) = \frac{2}{\pi}. \quad (14)$$

Note that, since K_β is not the actual renormalized stiffness, it does not necessarily vanish for $T > T_c$. However, in accordance with (13) we impose this fact by hand.

D. QMC simulation on Bose-Hubbard model

In order to validate the previously described approximations, we have carried *ab initio* QMC simulations of the Bose-Hubbard model, Eq.(1), using the worm algorithm.³⁸ Earlier work^{39,40} on isotropic 2D interacting Bose systems has shown that this algorithm can be used to study the KT transition. However, as pointed out by Prokof'ev and Svistunov in Ref.[41], the helicity modulus depends strongly on the aspect ratio of the lattice

employed in the QMC simulation, i.e. when the thermodynamic limit ($L_{x,y} \rightarrow \infty$) is taken by keeping L_x/L_y fixed in isotropic systems where $t_x = t_y$. As a result, the definition of superfluidity and its transition temperature can be different for different aspect ratios. The reason is that, as L_x/L_y is varied away from unity, the criticality of the system also undergoes a crossover from a classical 2D XY to 1D XY universality class. In the latter case, T_c and the helicity modulus vanish. The crossover would be complete when we are able to conduct simulations up to the thermodynamic limit. However, in finite systems finite-size effects prevent the system from completely reaching the 1D XY fixed point.

In this work, we focus on the effect of the hopping anisotropy, $\eta_0 = t_y/t_x \neq 1$, on the superfluid properties. Therefore, we must first determine a physically sensible prescription to obtain the helicity modulus and hence the BKT transition temperature. To this end, in our QMC simulations we have chosen a value of the system aspect ratio, L_x/L_y , such that the excitation energy of a unit quantized flux is the same in both directions in the noninteracting limit, i.e. $t_x \left(\frac{2\pi}{L_x}\right)^2 = t_y \left(\frac{2\pi}{L_y}\right)^2$ or $L_x/L_y = \sqrt{t_x/t_y}$. For example, for $t_y/t_x = 0.1$, we use $L_x = 100$ and $L_y = 32$ so that $L_x/L_y = 3.125 \simeq \sqrt{t_x/t_y} = \sqrt{10} = 3.1622$. The rationale for this choice is explained in what follows.

The helicity modulus can be defined as:^{42,43}

$$\gamma_{x,y} = \frac{2\Delta F(\phi_{x,y})}{\Omega(\phi_{x,y}/L_{x,y})^2}, \quad (15)$$

where $\Omega = L_x L_y$ is the system area and $\Delta F(\phi_{x,y})$ is the free energy change due to an infinitesimal phase twist $\phi_{x,y}$ applied at boundaries of the system. However, in a QMC simulation, the helicity modulus can be also obtained from the winding number fluctuations $\langle W_{x,y}^2 \rangle$:^{41,43}

$$\gamma_{x,y} = T \frac{L_{x,y}}{L_{y,x}} \langle W_{x,y}^2 \rangle, \quad (16)$$

where $\langle W_x^2 \rangle$ ($\langle W_y^2 \rangle$) are the winding-number fluctuations along x (y) direction.

In continuum systems, the helicity modulus, γ , can be related to a quantity with dimensions of density, namely the superfluid density ρ_s , by means of the equation:

$$\gamma = \frac{\hbar^2}{m} \rho_s \quad (17)$$

where m is the particle mass. In lattice systems, a natural generalization of (17) is obtained by replacing m by the effective mass, $m_{x,y}^*$, which may be direction dependent. Indeed, for free particles, $\frac{\hbar^2}{m_{x,y}^*} \sim 2t_{x,y}$, which implies that

$$\gamma_{x,y} = 2t_{x,y} \rho_s. \quad (18)$$

Therefore, the choice of aspect ratio $L_x/L_y = \sqrt{t_x/t_y}$ means (cf. Eq. 16) that $\langle W_x^2 \rangle = \langle W_y^2 \rangle$ and thus the superfluid density ρ_s alone determines the helicity modulus in both directions.

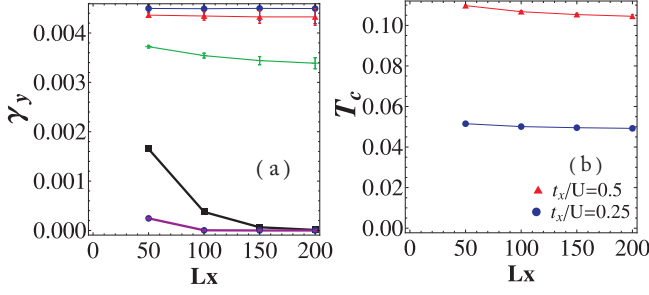


FIG. 3: (a) shows the helicity modulus in the y direction, γ_y obtained by QMC as a function of the longest side, L_x . We use $\eta_0 = J_y^0/J_x^0 = 0.02$, $t_x/U = 0.25$, and $\rho_0 \simeq 0.8$. From top to bottom lines are for $T/U = 0.01$ to 0.09 in steps of 0.02 . (b) T_c as a function of L_x for $\eta_0 = J_y^0/J_x^0 = 0.02$. $t_x/U = 0.5$, $\rho_0 \simeq 0.7$ for red triangles and $t_x/U = 0.25$, $\rho_0 \simeq 0.8$ for blue dots.

Next, let us assess the importance of finite size effects using the above choice for the system aspect ratio. In Fig. 3(a), we show the helicity modulus in the y direction, γ_y , as a function of the longest side, L_x , where $t_x/U = 0.25$, $\rho_0 \simeq 0.8$ and $\eta_0 = J_y^0/J_x^0 = 0.02$. By the variation of T/U from 0.01 to 0.09 , we find that, for $L_x \geq 100$ and $T \leq 0.05$, γ_y is almost unchanged. In Fig. 3(b), we show T_c as a function of L_x for $\eta_0 = J_y^0/J_x^0 = 0.02$. It can be seen that the variation of T_c (see Sec. III B for an explanation of how T_c is estimated from the QMC data) with L_x is less than 5%. These results justify that neglecting finite-size effects on the helicity modulus and T_c for the typical system sizes employed in our QMC simulations ($L_x > 100$).

III. SMALL TO INTERMEDIATE ANISOTROPY

A. Inside the Superfluid Phase

We first discuss the results of SCHA for the XY model, which approximates Eq. (2) by the Gaussian model of Eq. (5) with an effective quadratic coupling, $J_{ij}(T, U, n_0)$. The derivation of the equation for J_{ij} is given in Appendix A (cf. Eq. (A12)). We note that the non-linear Josephson term in Eq. (2) couples all Matsubara frequencies, and therefore, in SCHA, the renormalized J_{ij} in Eq. (5) acquires a temperature dependence.

From the continuum limit of the Gaussian model obtained from the SCHA (cf. Eq. 5), the helicity modulus can be read off: $\gamma_{x,y} = 2J_{x,y}$. Hence, we can also define anisotropy ratio as $\eta = \gamma_y/\gamma_x = J_y/J_x$. For later purposes, it is also worth introducing the *bare* (i.e. unrenormalized) system parameters: $\gamma_{x,y}^0 = 2J_{x,y}^0 = 2t_{x,y}\rho_0$ (ρ_0 is the mean lattice occupation and a the lattice parameter) and the bare anisotropy ratio $\eta_0 = \gamma_y^0/\gamma_x^0 = J_y^0/J_x^0 = t_y/t_x$. In what follows, we compare the results of $\gamma_{x,y}$ obtained from SCHA and QMC within anisotropic

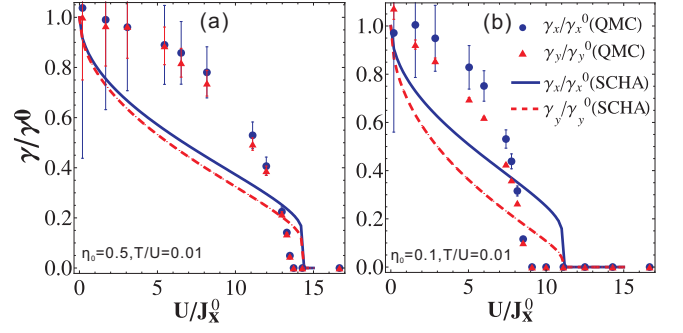


FIG. 4: The renormalized helicity modulus, $\gamma_\alpha/\gamma_\alpha^0$, as a function of the interaction strength, U/J_x^0 . Note that, on both figures, we keep constant the values of U , T , and $\eta_0 = J_y^0/J_x^0 = 0.5$ and 0.1 , and change J_x^0 . Blue solid (red dashed) lines represent the results in the $\alpha = x(y)$ directions. For comparison, we also show the numerical results obtained by QMC in filled circles and triangles together. See the text for more details of comparison.

superfluid (SF) phase.

In Fig. 4 we show the ratio of the renormalized to the bare helicity moduli, $\gamma_\alpha/\gamma_\alpha^0$ as a function of the interaction strength, U/J_x^0 . The bare anisotropy ratio parameter is chosen to be $\eta_0 = 0.5$ (Fig. 4(a)) and $\eta_0 = 0.1$ (Fig. 4(b)). Here we keep both U and T constant but change J_x^0 and J_y^0 in order to comparison with QMC data more easily. As expected, increasing the strength of interactions, that is, increasing U/J_x^0 , suppresses superfluidity as that both γ_x and γ_y decrease. Note that, within the SCHA, even a weak interaction can have a strong effect on the renormalized helicity modulus, $\gamma_{x,y}$. Indeed, when the interaction is larger than a critical value, the helicity modulus drops to zero in both directions discontinuously, and the system becomes a normal fluid without phase stiffness. This is a feature of the SCHA, which wrongly predicts the interaction-driven transition between the SF and the Normal fluid (which at $T = 0$ corresponds to the SF to Mott insulator quantum phase transition) to be of first order.

In the same figure, we also show numerical results of our QMC simulation for comparison. We can see that, although the ratio of the renormalized to the bare helicity modulus obtained from QMC exhibits qualitatively the same behavior as the SCHA, it does not show strong renormalization effects predicted by the SCHA at small U/J_x^0 . Furthermore, at larger U/J_x^0 , both γ_x/γ_x^0 and γ_y/γ_y^0 vanish rather smoothly.

In order to better understand how finite temperature and interactions influence the anisotropy ratio of the helicity modulus, we show in Fig. 5(a) and (b) the renormalized helicity ratio, $\eta = \gamma_y/\gamma_x$ vs. the bare one $\eta_0 = \gamma_y^0/\gamma_x^0 = t_y/t_x$. Results obtained both from the SCHA and QMC are shown together for comparison. We see that, at low temperatures ($T/U = 0.01$, Fig. 5(a)), when the system is deep in the superfluid phases, the anisotropy is barely renormalized, i.e. $\eta \simeq \eta_0$ and indeed

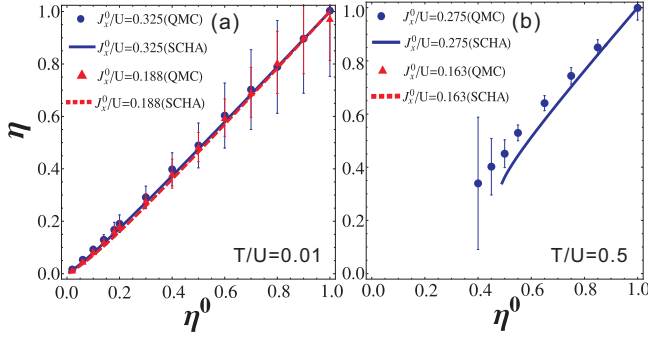


FIG. 5: Ratio of the renormalized helicity moduli, η vs. its bare (unrenormalized) value, η_0 , for (a) $T/U = 0.01$ and (b) $T/U = 0.5$. We choose different values of J_x^0/U : (a) $J_x^0/U = 0.325$ and $J_x^0/U = 0.188$ and (b) $J_x^0/U = 0.275$ and $J_x^0/U = 0.163$, and vary η_0 . Note that in (b), for $\eta_0 \lesssim 0.5$, the temperature is higher than the BKT transition temperature and therefore both γ_x and γ_y vanish. We also show the results of our QMC simulations for comparison. Both QMC and SCHa yield results in excellent agreement, suggesting that the anisotropy ratio of the helicity modulus is barely renormalized by interaction and finite-temperature effects. This is consistent with the SF phase being described by an isotropic Gaussian field theory, as discussed in Sec. II C.

our QMC results agree well with the SCHa predictions for η . Interestingly, this result holds also true at much higher temperatures (cf. Fig. 5(b)), except for the fact that, for small values of η_0 the system becomes a normal gas (i.e. the temperature used in the simulation $T/U = 0.5$ is larger than the BKT transition temperature, T_c , for these highly anisotropic systems). This is because as T_c of an anisotropic superfluid ($\eta_0 < 1$) becomes smaller, the renormalization of the helicity ratio also becomes more significant near the phase transition boundary. The agreement between SCHa and QMC results is very good.

Thus, we find that, although the SCHa and QMC yield different values for renormalized helicity moduli, γ_x and γ_y , QMC shows that the renormalized anisotropy ratio $\eta = \gamma_y/\gamma_x$ is barely affected by interaction and/or temperature effects. This is consistent with the SF phase being described, in the continuum limit, by an isotropic Gaussian field theory (cf. Eq. 10 in Sec. II C), which is also correctly captured by the SCHa.

B. Near the BKT transition

In Fig. 6, we show the helicity modulus (proportional to superfluid density, cf. Eq. 17) as a function of temperature. The bare single particle tunneling amplitude is $t_x/U = 0.5$ and $t_y/U = 0.25$ respectively, and the filling fraction is $\rho_0 \simeq 0.63$. In Fig. 6(a), the results of the helicity moduli obtained from the SCHa and QMC are compared. We thus see that, compared to the QMC results, the SCHa overestimates the temperature depen-

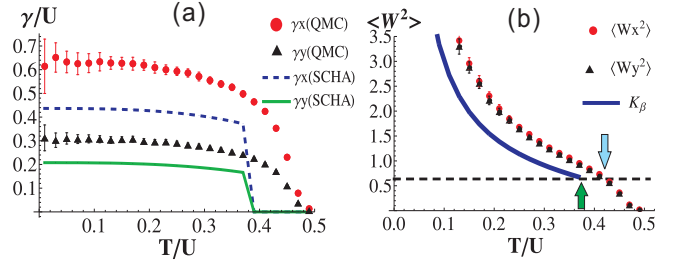


FIG. 6: The helicity modulus as a function of temperature for a fixed interaction U . The bare tunneling are $t_x/U = 0.5$, $t_y/U = 0.25$, and the density is $\rho_0 \simeq 0.63$. (a) shows results including interaction renormalization within SCHa, compared with the QMC results in dots and in triangulars. (b) shows the winding number fluctuation in QMC, and K_β obtained analytically from the SCHa to XY model, as a function of temperature. The horizontal dashed line indicate the universal number, $2/\pi$. The intersection of the curves (dots) and the horizontal lines gives the T_c in SCHa (QMC), marked by arrows.

dence of the helicity modulus in both directions roughly by a factor of one point five.

In Fig. 6(b), we show how the BKT transition temperature T_c is determined from both the analytical results of SCHa and the QMC data. In the case of the SCHa, we compute the phase stiffness as discussed in Sec. II C, i.e. from $K_\beta = \beta \sqrt{J_x J_y}$, where J_x and J_y are solutions to the SCHa equations for given T and U , J_x^0 , J_y^0 values. Hence, T_c is found by varying the temperature until $K_\beta = \frac{2}{\pi}$ (cf. Sec. II C).

As to the QMC data, T_c is obtained as follows: As anticipated in Sec. II D, by choosing $L_x/L_y = \sqrt{t_x/t_y}$ we find that the winding number fluctuations (red dots and black triangles in Fig. 6(b)) in the x and y directions essentially coincide. Furthermore, the $\langle W_{x,y}^2 \rangle$ show kink at a temperature, which is essentially equal to the one obtained by requiring that T_c (cf. Sec. II C):

$$K_\beta^{QMC}(T_c) = \frac{1}{T_c} \sqrt{\gamma_x(T_c) \gamma_y(T_c)} \\ = \sqrt{\langle W_x^2(T_c) \rangle \langle W_y^2(T_c) \rangle} \simeq \langle W_{x,y}^2 \rangle = \frac{2}{\pi} \quad (19)$$

where Eqs. (14) and (16) have been used. In Fig. 6(b), we have indicated the universal value of $\frac{2}{\pi}$ by a horizontal line. As explained in Sec. II C, in the SCHa, we assume that K_β vanishes for $T > T_c$. However, in the QMC calculations, finite-size effects round off the expected thermodynamic-limit discontinuity of K_β^{QMC} at $T = T_c$. Yet, as discussed in Sec. II D, the value of T_c estimated from the kink in the Monte Carlo data is converged for system sizes that we used ($L_x > 100$). Finally, the comparison of T_c as obtained from QMC and SCHa is shown in Fig. 8 and will be explained in more detail further below.

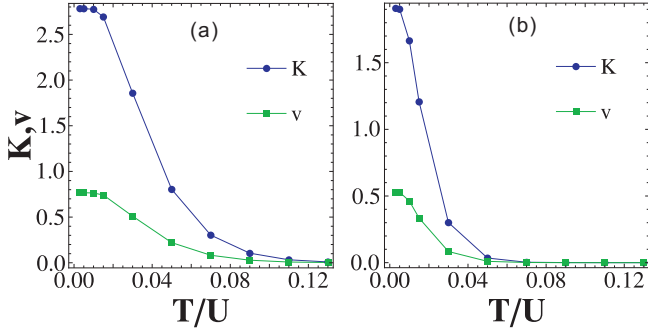


FIG. 7: The Luttinger parameters K and v as a function of the temperature, T/U . For the 1D Bose-Hubbard model, we fix $L_x = 150$ for both plots, and (a) $t_x/U = 0.5, t_y/U = 0, \rho_0 \simeq 0.7$ and (b) $t_x/U = 0.25, t_y/U = 0, \rho_0 \simeq 0.8$ respectively.

IV. LARGE ANISOTROPY

A. SCHA for the Coupled TLLs

To begin with, let us note that, for the 1D Bose-Hubbard model, the Luttinger parameters K and v that determine the properties of the TLLs in the decoupled limit (cf. Eq. 6 for $g_J^0 = 0$) cannot be analytically obtained for general lattice fillings and values of U/t_x (Eq. 1 for $t_y = 0$). Thus, in order to extract the Luttinger liquid parameter, K , and sound velocity, v , we have carried out additional QMC calculations for the 1D Bose-Hubbard model to extract these parameters. Using the relations $v/K = 1/\pi\kappa$ and $vK = \pi L_x T \langle W_x^2 \rangle$, where $\kappa = \partial\rho/\partial\mu$ is the compressibility and $\langle W_x^2 \rangle$ is the winding number fluctuation along the x direction for $T/U \ll 1$.⁴⁴ In Fig. 7 the numerical Luttinger parameters K and v as a function of the temperature are shown, T/U , for a large size of the 1D system of $L_x = 150$. The parameters characterizing one (decoupled) TLL correspond to the extrapolation of this results to very low temperature. Thus, for $T/U = 0.005$ we find $K \simeq 2.77$ and $v \simeq 0.77$ for $t_x/U = 0.5, \rho_0 \simeq 0.7$ in Fig. 7(a), and $K \sim 1.91, v \simeq 0.53$ for $t_x/U = 0.25, \rho_0 \simeq 0.8$ in Fig. 7(b).

Next, we describe the result of applying the SCHA to the system of coupled TLLs. Compared to the case of small anisotropy discussed above (Eq. A12), in this case only J_y is renormalized, and all the interaction dependence of J_y enters through the Luttinger parameters. However, as discussed in sec. II C, the system of coupled TLLs at finite temperature also belongs to the 2DXY universality class^{13,14}. Thus, the BKT critical temperature can be found from the equation:

$$K_\beta = 2 \frac{\sqrt{KvJ_y(T_c)/2\pi}}{T_c} = \frac{2}{\pi}, \quad (20)$$

In the SCHA calculations, we have chosen the short-distance cut-off such that $Kva_0/2\pi \simeq J_x$, when comparing the TLL-Gaussian model of Eq. (8) with the Gaussian model in Eq. (5).

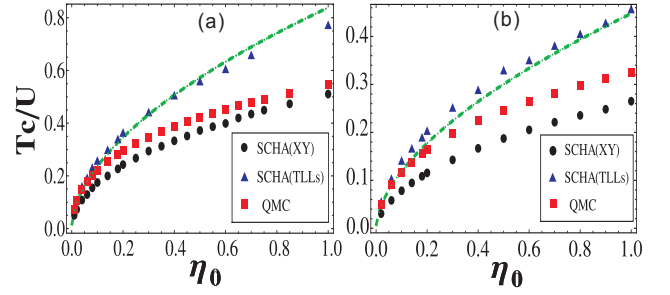


FIG. 8: T_c as a function of the bare anisotropy ratio, $\eta_0 = J_y^0/J_x^0 = t_y/t_x$ for $t_x/U = 0.5, \rho_0 \simeq 0.65 \pm 0.05$ ($J_x^0/U \simeq 0.325$) (a) and $t_x/U = 0.25, \rho_0 \simeq 0.75 \pm 0.05$ ($J_x^0/U \simeq 0.1825$) (b). The blue triangles are the results obtained by SCHA to the XY model. The black dots correspond to the results obtained by SCHA to an array of coupled TLLs. The Red squares are the QMC data. T_c is determined by the methods discussed in Section III B. On both panels, the green dash curve is a fit to the scaling behavior of T_c with the bare anisotropy ratio η_0 yielding $T_c/U \simeq 0.837\eta_0^{0.55}$ (a) $T_c/U \simeq 0.448\eta_0^{0.575}$ (b).

In Fig. 8 (black dots), we show the BKT critical temperature, T_c computed using the SCHA, and QMC as a function of the bare anisotropy ratio. As discussed above, T_c goes to zero gradually as the bare anisotropy ratio η_0 becomes larger, reflecting the fact that there is no superfluid phase transition at finite temperature in 1D system. From both panels in Fig. 8, it can be seen that the SCHA to XY model provides a reasonably good description of T_c (compared to the QMC results) for $\eta_0 \approx 1$ and weak interactions (Fig. 8(a)), but it deviates from the QMC results for stronger interactions (Fig. 8(b)) and small η_0 . On the other hand, the results obtained by applying the SCHA to an array of coupled TLLs are found to be closer to the QMC results for T_c in the large anisotropy regime (i.e. small η_0). These results are consistent with the expectation that the SCHA to the XY model should be more accurate in the small anisotropy regime, whereas applying the SCHA to an array of coupled TLLs becomes a better approximation in the limit of large anisotropy.

B. RG scaling for critical temperature

Besides of the numerical calculations of BKT critical temperature, from our QMC data we can also extract the scaling behavior of T_c with anisotropy ratio η_0 . This can be compared with the results obtained by the renormalization group flow of the Josephson coupling in Eq (7), which described by the differential equation:^{13,14}

$$\frac{dg_J}{d\ell} = \left(2 - \frac{1}{2K}\right) g_J. \quad (21)$$

where the flow parameter $\ell = \ln(a(\ell)/a_0) = \ln(\Lambda(0)/\Lambda(\ell))$, with $a(\ell) = a_0 e^\ell$. Since $K \in [1, +\infty)$ for the Bose-Hubbard model is far from the critical point $K^* = 1/4$, we can neglect the renormalization of K and

treat it as a constant.^{13,14} Therefore, the solution to (21) reads $g_J(\ell) \simeq g_J(0)e^{(2-\frac{1}{2K})\ell}$. To complete the solution, we need to recall that the bare (energy) cut-off $\Lambda(0) \approx t_x$, and $g_J(0) \simeq 2\pi t_y \rho_0 a_0^2/v$. In order to estimate of the critical temperature at which the system will enter the SF phase, we note that, at finite temperatures, the RG flow is cut off at the scale $\Lambda(\ell) \simeq T$, and $g_J(T = T_c) \sim 1$. Hence, provided (21) provides accurate description of the entire flow (i.e. for small enough $g_J(0)$), we have

$$T_c \simeq C\eta_0^{\frac{1}{2-1/2K}} = C\eta_0^{\frac{2K}{4K-1}} \quad (22)$$

where C is a prefactor that depends on microscopic details of the model, and can be obtained by fitting above scaling law to the QMC results. It is worth noting that¹⁴ the same scaling law for T_c/t_x with η_0 can be also obtained using mean-field theory, i.e. by assuming that $\langle e^{i\theta_n(0)} \rangle = \phi_0(T)$. However, as discussed in the Introduction, strictly speaking mean-field theory is inapplicable in two dimensions due to the lack of BEC at finite temperatures.

In Fig. 8 we use the values of the Luttinger parameters obtained earlier from QMC simulations of the 1D Bose-Hubbard model ($K \simeq 2.77$ and $v \simeq 0.77$ in Fig. 8(a) and $K \sim 1.91$, and $v \simeq 0.53$ in Fig. 8(b)) to fit the scaling of T_c . In particular, the value of K completely determines the exponent of the scaling law (cf Eq.22), and thus, the only free parameter is the prefactor C . The fit yields $T_c/U \simeq 0.837\eta_0^{0.55}$ for the data on Fig. 8(a) and $T_c/U \simeq 0.448\eta_0^{0.575}$ for the data on Fig. 8(b). Using the TLLs parameters obtained from $T/U = 0.005$, the predicted T_c of SCHa to TLLs are close to QMC calculations at large anisotropy regimes.

V. CONCLUSION

In summary, two different approaches, the SCHa and QMC, reveal the highly nontrivial features of the helicity modulus and the BKT phase transition in the 2D Bose-Hubbard model with anisotropic hopping. These characteristic features simulated by QMC using a specific system aspect ratio, $L_x/L_y = \sqrt{t_x/t_y}$, is consistent with the rescaling of the effective sine-Gordon model. We show how the interaction and finite temperature effect influence the helicity modulus and find profound agreement of anisotropy of the helicity modulus given by the SCHa and QMC. As we drive the system towards the extremely anisotropic limit, the BKT transition temperature approaches to the absolute zero and the transition thus becomes a 3DXY quantum critical point at the end of a line of classical 2DXY critical points. In particular, through the RG scheme for the coupled TLLs, we obtain the scaling relation of T_c with anisotropy ratio. Employing ultra-cold atoms in a controllable optical lattice opens avenues to identify our results of 2D anisotropic Bose-Hubbard model.

VI. ACKNOWLEDGEMENT

This work is supported by NSC grants and NCTS at the same time. MAC gratefully acknowledges the hospitality of NCTS (Taiwan) and the financial support of the Spanish MEC through grant FIS2010-19609-C02-02.

Appendix A: Self-consistent Harmonic Approximation

To find the optimally quadratic approximation to the XY-model, we employ the self-consistent Harmonic approximation (SCHa). In this approach, the action of XY or quantum rotor model, Eq. (2), is approximated by an anisotropic Gaussian model:

$$\begin{aligned} S_G[\theta] &= \int_0^\beta d\tau \left\{ \sum_i \frac{(\partial_\tau \theta_i)^2}{2U} + \sum_{\langle i,j \rangle} J_{ij}(\theta_i - \theta_j)^2 \right\} \\ &= \frac{1}{2} \sum_{\mathbf{k}, \omega_n} G_v^{-1}(\mathbf{k}, \omega_n) |\theta(\mathbf{k}, \omega_n)|^2, \end{aligned} \quad (A1)$$

where $\omega_n = 2\pi Tn$, and the single particle Green's function is given by

$$G_v^{-1}(\mathbf{k}, \omega_n) = \frac{\omega_n^2}{U} + \sum_\alpha 8J_\alpha \sin^2(k_\alpha \hat{a}_\alpha/2). \quad (A2)$$

Next, we make use of Feynman's variational principle, which states that:

$$F = -\frac{1}{\beta} \ln Z \leq \tilde{F}[G_v] = F_v + \frac{1}{\beta} \langle S[\theta] - S_G[\theta] \rangle_v, \quad (A3)$$

where $\langle \rangle_v$ denotes the average with respect to $S_G[\theta]$ and S is the XY model action. Since

$$e^{-\beta F_v} = \int D\theta e^{-S_v[\theta]} = \prod_{\mathbf{k}, \omega_n} G_v(\mathbf{k}, \omega_n)^{-1/2}, \quad (A4)$$

the first term of $\tilde{F}[G_v]$ is:

$$F_v = -\frac{1}{2\beta} \sum_{\mathbf{k}, \omega_n} \ln G_v(\mathbf{k}, \omega_n). \quad (A5)$$

The remaining contributions to $\tilde{F}[G_v]$ are

$$\begin{aligned} &\langle S_{xy}[\theta] - S_G[\theta] \rangle_v \\ &= \langle \int_0^\beta d\tau \left\{ \sum_i \frac{1}{2U} (\partial_\tau \theta_i)^2 - \sum_{\langle i,j \rangle} 2J_{ij}^0 \cos(\theta_i - \theta_j) \right\} \rangle_v \\ &\quad - \langle S_G[\theta] \rangle_v \\ &= \sum_{\mathbf{k}, \omega_n} \frac{\omega_n^2}{2U} G_v(\mathbf{k}, \omega_n) + \langle S_{\cos} \rangle_v - \text{const.} \end{aligned} \quad (A6)$$

with

$$\langle S_{\cos} \rangle_v = - \int_0^\beta d\tau \sum_{\langle i,j \rangle} 2J_{ij}^0 \langle \cos(\theta_i - \theta_j) \rangle_v.$$

Hence,

$$\begin{aligned}\langle \cos(\theta_i - \theta_j) \rangle_v &= \text{Re} \left[e^{-\frac{1}{2} \langle (\theta_i - \theta_j)^2 \rangle_v} \right] \\ &= \text{Re} \left[G_v(r_i - r_j, 0) - G_v(0, 0) \right], \quad (\text{A7})\end{aligned}$$

by the cumulant expansion. Here

$$G_v(r, \tau) = \frac{1}{\beta \Omega} \sum_{\mathbf{k}, \omega_n} e^{i\mathbf{k}r} e^{-i\omega_n \tau} G_v(\omega_n, \mathbf{k}),$$

is the single particle Green's function in real space. Therefore we have,

$$\begin{aligned}\langle S_{\cos} \rangle_v &= - \int_0^\beta d\tau \sum_{\langle i, j \rangle} 2J_{ij}^0 \text{Re} \left[e^{G_v(r_i - r_j, 0) - G_v(0, 0)} \right] \\ &= -\beta \sum_i \sum_{\mathbf{t}=\hat{a}_x, \hat{a}_y} 2J_{\mathbf{t}}^0 \text{Re} \left[e^{G_v(\mathbf{t}, 0) - G_v(0, 0)} \right] \\ &= -\beta \Omega \sum_{\alpha} 2J_{\alpha}^0 \text{Re} \left[e^{\frac{1}{\Omega \beta} \sum_{\mathbf{k}, \omega_n} (e^{i\mathbf{k} \cdot \hat{a}_\alpha} - 1) G_v(\mathbf{k}, \omega_n)} \right]. \quad (\text{A8})\end{aligned}$$

Upon combining above results and finding the extrema of $\tilde{F}[G_v]$, i.e.

$$\frac{\delta F'[G_v]}{\delta G_v(\mathbf{k}, \omega_n)} = 0, \quad (\text{A9})$$

we find

$$\begin{aligned}& \frac{1}{G_v(\mathbf{q}, \omega_n)} \\ &= \frac{\omega_n^2}{U} + 8 \sum_{\alpha} J_{\alpha}^0 \sin^2(q_{\alpha} \hat{a}_{\alpha}/2) e^{\frac{1}{\Omega \beta} \sum_{\mathbf{k}, \omega_n} (e^{i\mathbf{k} \cdot \hat{a}_{\alpha}} - 1) G_v(\mathbf{k}, \omega_n)} \\ &\equiv \frac{\omega_n^2}{U} + 8 \sum_{\alpha} J_{\alpha} \sin^2(q_{\alpha} \hat{a}_{\alpha}/2). \quad (\text{A10})\end{aligned}$$

Using the Matsubara sum

$$\begin{aligned}\frac{1}{\beta} \sum_{\omega_n} G_v(\mathbf{k}, \omega_n) &= \frac{U}{\beta} \sum_{\omega_n} \frac{1}{\omega_n^2 + \omega_{\mathbf{k}}^2} \\ &= \frac{U}{2\omega_{\mathbf{k}}} \coth\left(\frac{\beta\omega_{\mathbf{k}}}{2}\right), \quad (\text{A11})\end{aligned}$$

we conclude that

$$\ln \frac{J_{\alpha}}{J_{\alpha}^0} = \frac{1}{\Omega} \sum_{\mathbf{k}} (e^{i\mathbf{k} \cdot \hat{a}_{\alpha}} - 1) \frac{U}{2\omega_{\mathbf{k}}} \coth\left(\frac{\beta\omega_{\mathbf{k}}}{2}\right). \quad (\text{A12})$$

Note that $\omega_{\mathbf{k}} = 2\sqrt{2U} \sqrt{J_x \sin^2(k_x a/2) + J_y \sin^2(k_y a/2)}$ is the phonon (Bogoliubov) excitation energy.

Appendix B: SCHA for Coupled TLLs

Applying the methods of previous section to the action of Eq. (7), the following equation for the renormalized parameter $J_y (= g_J v / \pi a_0^2)$ is obtained:

$$\ln \frac{g_J}{g_J^0} = \frac{v K^{-1}}{L_x L_y} \sum_{\mathbf{k}} \frac{e^{i\mathbf{k} \cdot \hat{\mathbf{y}}} - 1}{\omega_{\mathbf{k}}} \coth\left(\frac{\beta\omega_{\mathbf{k}}}{2}\right), \quad (\text{B1})$$

where $\omega_{\mathbf{k}} = 2\sqrt{v^2(k_x/2)^2 + \frac{2\pi v J_y}{K} \sin^2(k_y/2)}$.

- ¹ M. Greiner, O. Mandel, T. Esslinger, T. W. Hansch and I. Bloch, *Nature (London)* **415**, 39 (2002).
- ² D. Jaksch, C. Bruder, J. I. Cirac, C. W. Gardiner, and P. Zoller, *Phys. Rev. Lett.* **81**, 3108 (1998).
- ³ I Bloch, J. Dalibard, and W. Zwerger, *Rev. Mod. Phys.* **80**, 885-964 (2008).
- ⁴ T. Stöferle *et al.* *Phys. Rev. Lett.* **92**, 130403 (2004)
- ⁵ Chen-Lung Hung, Xibo Zhang, Nathan Gemelke, and Cheng Chin, *Nature (London)* **470**, 236 (2011).
- ⁶ S. Trotzky, L. Pollet, U. Schnorrberger, F. Gerbier, I. Bloch, N. V. Prokof'ev, B. Svistunov, and M. Troyer, *Nature Phys.* **6**, 998 (2010).
- ⁷ X. Zhang, C.-L. Hung, S.-K. Tung, and C. Chin, *arXiv:1109.0344* (2011).
- ⁸ E. Haller *et al.* *Nature (London)* **466**, 597 (2010)
- ⁹ C. Becker *et al.*, *New J. of Phys.* **12** 065025 (2010).
- ¹⁰ Z. Hadzibabic, P. Kruger, M. Cheneau, B. Battelier, and

- J. Dalibard, *Nature (London)* **441**, 1118 (2006).
- ¹¹ M. A. Cazalilla, A. Iucci, and T. Giamarchi, *Physical Review A* **75**, 051603(R) (2007).
- ¹² L. M. Mathey, A. Polkovnikov, and A. H. Castro-Neto, *Europhysics Letters*, **81**, 10008 (2008).
- ¹³ A. F. Ho, M. A. Cazalilla, and T. Giamarchi, *Phys. Rev. Lett.* **92**, 130405 (2004).
- ¹⁴ M. A. Cazalilla, A. F. Ho, and T. Giamarchi, *New J. Phys.* **8**, 158 (2006).
- ¹⁵ V. Cataudella and P. Minnaghen, *Physica (Amsterdam)* **C166**, 442 (1990).
- ¹⁶ B. Chattopadhyay and S. R. Shenoy, *Phys. Rev. Lett.* **72**, 400 (1994).
- ¹⁷ P. Minnaghen and P. Olsson, *Phys. Rev. B* **44**, 4503 (1991).
- ¹⁸ L. Benfatto, C. Castellani, and T. Giamarchi, *Phys. Rev. Lett.* **98**, 117008 (2007).
- ¹⁹ O. A. Starykh and L. Balents, *Phys. Rev. Lett.* **98**, 077205 (2007).

- ²⁰ M. Kohno, O. A. Starykh and L. Balents, *Nature Phys.* **3**, 790 (2007).
- ²¹ T. Giamarchi, Ch. Regg, O. Tchernyshyov, *Nature Phys.* **4**, 198 (2008).
- ²² Ch. Rüegg *et al.* *Phys. Rev. Lett.* **101**, 247202 (2008); P. Bouillot *et al.*, *Phys. Rev. B* **83**, 054407 (2011).
- ²³ W. P. Su, J. R. Schrieffer, and A. J. Heeger, *Phys. Rev. Lett* **42**, 1698 (1979); D. C. Tsui, H. L. Stömer, and H. C. Gossard, *Phys. Rev. Lett.* **48**, 1559 (1982); R. B. Laughlin, *Phys. Rev. Lett.* ; D. Arovas, J. R. Schrieffer, and F. Wilczek, *Phys. Rev. Lett.* **53**, 722 (1984).
- ²⁴ M. A. Cazalilla, R. Citro, T. Giamarchi, E. Orignac, M. Rigol, *Rev. Mod. Phys.* **83**, 1405-1466 (2011) .
- ²⁵ J. M. Kosterlitz and D. J. Thouless, *J. Phys. C* **6**, 1181 (1973).
- ²⁶ Bishop and Reppy, *Phys. Rev. Lett.* **40**, 1727 (1978).
- ²⁷ D. Gangardt, P. Pedri, L. Santos, and G. Shlyapnikov, *Phys. Rev. Lett.* **96**, 040403 (2006).
- ²⁸ S. Bergkvist *et al.* *Phys. Rev. Lett.* **99**, 110401 (2007); M. Rehn *et al.* *Eur. Phys. J. D* **49**, 223 (2008)
- ²⁹ J. K. Freericks, *Phys. Rev. A* **78**, 013624 (2008)
- ³⁰ J. Taniguchi, Y. Aoki, and M. Suzuki, *Phys. Rev. B* **82**, 104509 (2010); J. Taniguchi, R. Fujii, and M. Suzuki, *Phys. Rev. B* **84**, 134511 (2011).
- ³¹ D. R. Nelson and J. M. Kosterlitz *Phys. Rev. Lett.* **39**, 1201(1977).
- ³² T. Giamarchi and B. S. Shastry, *Phys. Rev. B* **51**, 10915 (1995).
- ³³ A. Del Maestro and I. Affleck, *Physical Review B* **82**, 060515(R) (2010).
- ³⁴ T. Eggel, M. A. Cazalilla, M. Oshikawa, *Phys. Rev. Lett.* **107**, 275302 (2011).
- ³⁵ R. P. Feynman. *Statistical Mechanics*.
- ³⁶ J. V. Jose *et al.*, *Phys. Rev. B* **16**, 1217(1977).
- ³⁷ Naoto Nagaosa, *Quantum Field Theory in Condensed Matter Physics*.
- ³⁸ L. Pollet, K. Van Houcke and S. M.A. Rombouts, *J. Comp. Phys.* **225**, 2249-2266 (2007).
- ³⁹ Barbara Capogrosso-Sansone, Şebnem Güneş Soyluer, Nikolay Prokof'ev, and Boris Svistunov, *Phys. Rev. A* **77**, 015602 (2008)
- ⁴⁰ Lode Pollet, Corinna Kollath, Kris Van Houcke, and Matthias Troyer, *New J. Phys.* **10**, 065001 (2008)
- ⁴¹ N.V. Prokof'ev and B.V. Svistunov, *Phys. Rev. B* **61**, 11282 (2000).
- ⁴² Michael E. Fisher, Michael N. Barber and David Jasnow, *Phys. Rev. A* **8**, 1111 (1973)
- ⁴³ E. L. Pollock and D. M. Ceperley, *Phys. Rev. B* **36**, 8343(1987)
- ⁴⁴ M. A. Cazalilla, *Journal of Physics B: AMOP* **37**, S1-S47 (2004)